Polymers in disordered environments

Niklas Fricke, Sebastian Sturm, Marc Lämmel, Sebastian Schöbl, Klaus Kroy*, Wolfhard Janke#

Institute for Theoretical Physics, Universität Leipzig, Leipzig, Germany
*klaus.kroy@uni-leipzig.de, #wolfhard.janke@itp.uni-leipzig.de

Abstract

Using a combination of analytical theory and newly developed numerical algorithms, we analyze the most pertinent conformational characteristics of three paradigmatic types of polymers in disordered environments: (i) flexible polymers in quenched, self-similar disorder as represented by a self-avoiding random walk on a critical percolation cluster, (ii) semiflexible polymers in quenched, steric disorder as represented by an equilibrium hard-disk fluid and (iii) semiflexible polymers subject to the random energy landscape that emerges from a surrounding network of similar semiflexible polymers.

Keywords: Polymers in disorder, self-avoiding walks, percolation clusters, exact enumerations, semiflexible polymers in crowded environments, hard-disk fluid, chain-growth computer simulations, tube model of semiflexible polymers

1   Introduction

The world of biopolymers is crowded and disordered. From actin filaments and microtubules in the cytoskeleton to DNA strands in the nucleus—their environments are highly inhomogeneous, often across many length scales [1]. To the macroscopic observer, these inhomogeneities make themselves felt by modulating the material response to external stresses, whereas to a polymer embedded within, inhomogeneities chiefly appear as a constraint on its conformational fluctuations. Conversely, if the impact of environmental disorder on single-polymer statistics is well understood, the diffusive shape fluctuations of disorder-embedded polymers can be used as a local probe of the material microstructure, complementing the coarse-grained view afforded by macroscopic response measurements. Understanding the impact of disorder on the polymers' statistics and dynamics is therefore an important problem in modern polymer physics. We approach the topic from complementary angles by focusing on the two most common types of biopolymers, *flexible* polymers such as tropocollagen [2] and *semiflexible* polymers such as F-actin or microtubules [3].

Flexible polymers offer little to no mechanical resistance to external forces. Every possible conformation is thus equally likely in equilibrium, constrained only by the fact that polymers are unable to self-intersect. This endows flexible polymers with the equilibrium properties of a "self-avoiding random walk" (SAW) such as a mean square end-to-end distance $\langle R^2 \rangle$ that scales slightly superdiffusively in
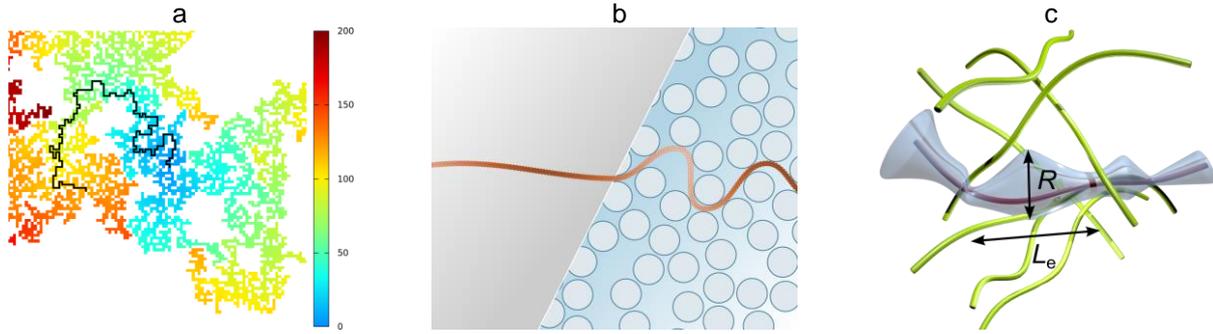
Figure 1: (a) Self-avoiding walks on a critical percolation cluster achieve a larger overall extension on average than SAWs in free space. Here shown is a typical conformation of a 200-step SAW on a *2d* cluster. The coloring reflects the shortest-path distance of cluster sites to the origin (center). (b) Semiflexible polymers exposed to a quenched hard-disk fluid background (right) bend more strongly than their unconstrained counterparts in free space (left). The resulting conformational statistics can be captured using an effective WLC model with a renormalized persistence length. (c) Network effects on a test polymer in semidilute solution can be described by a confinement tube. Its radius R varies along the polymer contour with a characteristic correlation length L_e representing the distance between mutual collisions with neighboring background chains.

the number of monomers N and an algebraic correction to the partition sum Z,

$$\langle \boldsymbol{R}^2 \rangle \sim N^{2\nu}, \nu > 1/2, \quad \text{and} \quad Z \sim \mu^N N^{\gamma-1}, \tag{1}$$

where ν and γ are universal critical exponents. For a flexible polymer living on the random fractal landscape of a percolation cluster, as illustrated in Figure 1, it had long been conjectured (see [4] and references therein) that the disorder averaged analogues of these quantities obey similar scaling relations, albeit with different exponents,

$$\overline{\langle \boldsymbol{R}^2 \rangle} \sim N^{2\bar{\nu}}, \quad \text{and} \quad \bar{Z} \sim \bar{\mu}^N N^{\bar{\gamma}-1}. \tag{2}$$

Extensive numerical work on the subject [4, 5, 6] has provided convincing evidence for the power-law growth of $\overline{\langle \boldsymbol{R}^2 \rangle}$, but not for the expected scaling behavior of $\bar{Z}$. We have developed a new exact enumeration algorithm that is vastly more efficient than conventional numerical tools [7, 8]. Using our new algorithm, we have determined the scaling exponent $\bar{\nu}$ to unprecedented precision and could furthermore show that $\bar{Z}$ obeys a different scaling law than hitherto assumed, see sections 2 and 3.

In contrast to flexible polymers, semiflexible polymers possess a finite internal bending rigidity κ that allows them to withstand external forces. Their energetic ground state is that of a rigid rod and deviations from the ground state are governed by the Wormlike Chain (WLC) Hamiltonian, which penalizes backbone curvature $|\partial_s^2 \boldsymbol{r}|$ (where $\boldsymbol{r}(s)$ denotes the continuous, arclength-parametrized polymer contour),

$$\mathcal{H} = \frac{\kappa}{2} \int_0^L |\partial_s^2 \boldsymbol{r}(s)|^2 \mathrm{d}s. \tag{3}$$

It follows from Eq. (3) that the tangents $\boldsymbol{t}(s) \equiv \partial_s \boldsymbol{r}(s)$ to the contour decorrelate exponentially in thermal equilibrium,

$$\langle \boldsymbol{t}(s) \cdot \boldsymbol{t}(0) \rangle = \exp(-s/\ell_p). \tag{4}$$

The *persistence length* ℓ_p ordinarily depends on the bending rigidity κ, the temperature T, and the dimensionality d of the embedding space,

$$\ell_p = \frac{2}{d-1}\frac{\kappa}{k_{\mathrm{B}}T},$$

(5)

but little is known about how ℓ_p changes or whether a persistence length in the strict sense defined via Eq. (4) even exists in the presence of disorder. Using a newly developed growth algorithm, we numerically simulated semiflexible polymers embedded in the background of a quenched hard-disk fluid that serves as a paradigmatic model for molecular crowding within the cytoskeleton. We showed that the disorder averaged tangent-tangent correlation function still decays exponentially, albeit with a renormalized persistence length ℓ_p^* [9]. We furthermore found that ℓ_p^* relates to the thermal persistence length ℓ_p via an auxiliary quantity that depends only on properties of the environmental disorder and thus defines a novel quantitative measure of molecular crowding, see section 4.

Semiflexible polymer *networks* such as the cytoskeletal actin cortex constitute another important class of environmental disorder. Due to its filamentous structure, this type of environment allows for virtually unimpeded motion along the polymer backbone but strongly constrains lateral motion. On intermediate time scales, the transverse deviations $\boldsymbol{r}_\perp$ of a single test polymer from its mean backbone axis thus trace out a "tube" that can be approximated analytically by adding to the WLC Hamiltonian a harmonic confinement term,

$$\mathcal{H} = \int_0^L \left[\frac{\kappa}{2} |\partial_s^2 \boldsymbol{r}(s)|^2 + \frac{\varphi}{2} |\boldsymbol{r}_\perp(s)|^2 \right] \mathrm{d}s.$$

(6)

Traditionally, φ has been considered constant along the polymer backbone, despite the strong inhomogeneities that can be observed in real polymer networks [10]. To address the statistics of the tube strength φ, we developed a systematic theory [11] which, based on a binary collision approximation, describes fluctuations of φ in an entangled polymer solution on the scale of individual tube collisions [12]. This approach allows us to determine the local tube radius $R(s)$, defined through

$$R^2(s) \equiv \frac{1}{2}\langle \boldsymbol{r}_\perp^2(s) \rangle,$$

(7)

and its statistical distribution function $P(R)$. The shape of $P(R)$, which is found to be given by a universal, non-Gaussian scaling function with a stretched tail, compares well with experimental data for F-actin solution of various concentrations.

The remaining article is organized as follows: Section 2 outlines a new algorithm for exact enumeration of SAWs on critical percolation clusters. Results for their asymptotic scaling behavior obtained by this method are subsequently discussed in section 3. We then turn to semiflexible polymers modeled by the WLC: Section 4 presents numerical and analytical findings concerning the effect of quenched disorder in the form of a hard-disk fluid on the chain's persistence length and tangent-tangent correlation function, while section 5 discusses the situation of a polymer being part of a random network via the "tube model". Our main findings and conclusions are summarized in section 6.

2   Scale-free enumeration of SAWs on percolation clusters

There are two numerical strategies to treat SAWs on a percolation cluster, namely exact enumeration and chain-growth Monte Carlo sampling. Among the latter class of methods, the pruned-enriched Rosenbluth algorithm (PERM) [13] is best suited to the problem, allowing for a few hundred steps with manageable effort [6]. For longer chains, however, its estimates become unreliable as it struggles to properly sample the clusters' rugged landscapes [14]. Exact enumeration is usually restricted to much shorter chains still, about forty or fifty steps depending on the dimension [5, 15], due to exponential increase of conformations and thus computation time. As we have recently shown [7], however, this can be overcome by a suitable factorization of the problem that exploits an intrinsic hierarchical structure. Since critical percolation clusters are finitely-ramified fractals, see [16], regions ("cells") of any size can be disconnected by removing a small number of sites (or bonds). This can be utilized in the following way: We partition the cluster into a hierarchy of nested cells, each having a small number of connections to its "parent" and "children"; see Figure 2. Rather than generating all SAW conformations on the whole cluster, we then successively construct the segments through each cell in turn, starting at the bottom of the hierarchy. The crux is that when we generate the segments through a cell, its children can be treated as single sites. The number of segment conformations and the average end-to-end distances are then obtained by multiplying each path with the number of different possibilities to traverse the child. This factorizes the number of required operations, allowing thus, if repeatedly applied over all length scales, to reduce the exponential complexity of exact enumeration to polynomial.

Interestingly, the exponent characterizing the complexity of the enumeration is practically identical in $2d$ and $3d$, with a value of roughly 2.4. This can be seen in Figure 3, where the average runtime for the scale-free enumeration (SFE) procedure is plotted as a function of the number of steps N as well as the time needed for partitioning the cluster. The gain in efficiency implied by this reduction to polynomial complexity is not easily grasped: Enumerating all conformations of a 10^4-step SAW (typically about 10^{1550} on a $2d$ cluster) would take over 10^{1500} ages of the universe using the standard enumeration method – our SFE procedure does it in about twenty minutes. However, this is only possible if the cluster is properly partitioned into a hierarchy that reflects its connectivity, which poses a major challenge. Note that there is no unique solution to this; a poor partitioning will still work in principle but (dramatically) inflate time and memory required for the enumeration. We tackled the problem via an amalgamation algorithm, where small pieces of the cluster are repeatedly fused to form larger ones in such a way that the resulting number of external connections is kept low. A more detailed description of this may be found elsewhere [17].

While the basic ideas underlying the SFE method are relatively simple, its implementation is rather complex and prone to errors. To ensure that it operates correctly, we always verify the results for the initial thirty steps using the standard method. In addition, we compared results for systems of medium size against those generated by PERM with very high statistics [14]. Finally, the non-uniqueness of the partitioning provides a way to check the method's correctness by comparing results obtained with different hierarchies. This test was successfully carried out for a sample of several thousand of the largest systems.
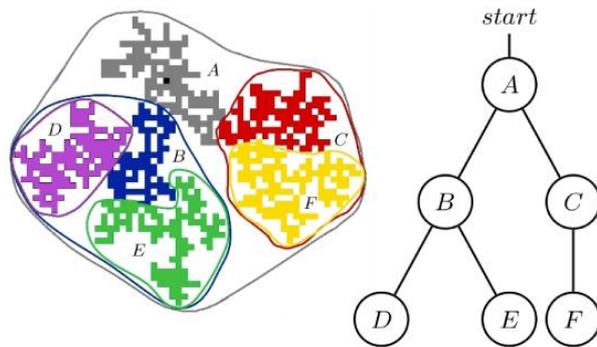
Figure 2: Partitioning of a critical percolation cluster into nested cells and corresponding tree hierarchy. The black spot within the gray cell *A* marks the starting position of the walks. Reproduced from Ref. [7].
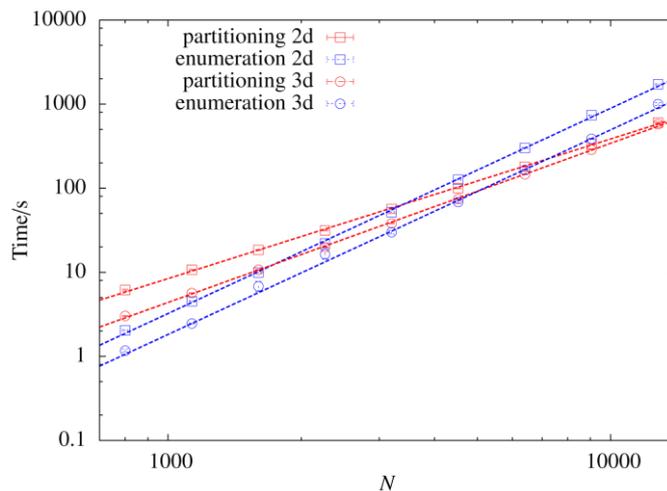
Figure 3: Average runtime (in seconds) for partitioning the clusters (red) and enumeration of the SAWs (blue) in two and three dimensions (squares and circles, respectively) on a log-log scale. Each data point was obtained from a sample of 10^3 clusters. The dashed lines correspond to least-squares power-law fits.

The scale-free enumeration method can be extended to accommodate nearest-neighbor interactions and can hence also be applied to investigate self-interacting self-avoiding walks (SASAWs). Here the exact nature of the results is particularly valuable, as it gives access to the full temperature spectrum. The results of these investigations shall be discussed in a forthcoming publication [18].

3   Asymptotic scaling behavior of flexible polymers in disorder

To uncover the dependence of the quenched average of the end-to-end distance and the number of conformations on the number of steps, we enumerated SAWs of different length on independent random disorder samples, each consisting of at least 5×10^4 clusters. In $3d$ we went up to a maximum of $N =$ 12800 steps, while we have so far only analyzed walks of up to $N = 1000$ steps in $2d$. The results for the $3d$ case are plotted in Figure 4 on a double-logarithmic scale, where the values were scaled by $N^{1.33} \approx N^{2\overline{\nu}}$ for the sake of visibility. The plot also shows results obtained using the cluster *backbones*, those structures which remain if all singly-connected *dangling ends* are removed. As can be seen, the slope on the backbones agrees asymptotically with that on full clusters, resolving a longstanding controversy [19, 20, 6, 7]. Initially, however, it is markedly larger as it takes about $N = 800$ steps for the asymptotic behavior to manifest itself. Using $N = 800$ as *lower* cutoff for a simple least-squares fit, we
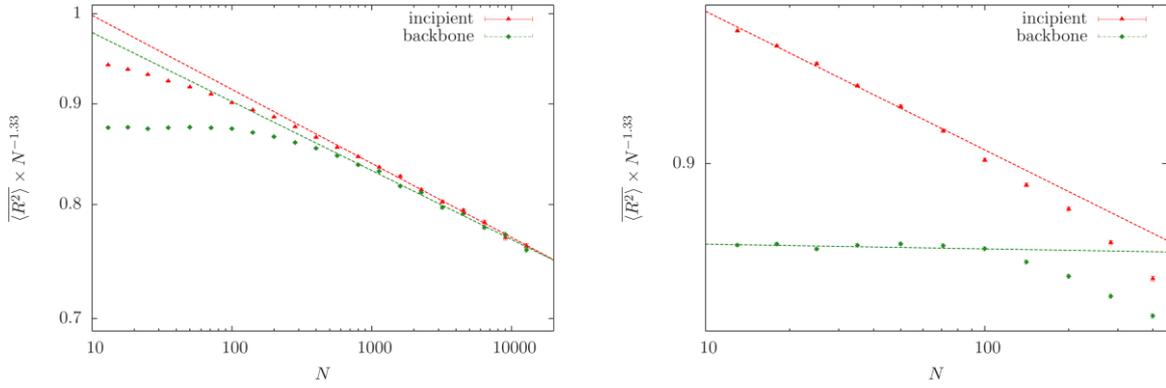
Figure 4: Mean squared end-to-end distance vs. number of steps for SAWs on incipient critical clusters (red) and backbones (green) on a log-log scale. The lines show the results from different least-square fits over the intervals $N = 800$–12800 (left) and $N = 13$–84 (right). The factor $N^{-1.33}$ ($\approx N^{-2\nu}$) serves to magnify the differences. Reproduced from Ref. [8].

obtained the estimate $\bar{\nu}_{3d} = 0.6433(4)$. The fact that this value is significantly smaller than estimates from previous analyses of smaller systems (0.662(6) [5] and 0.667(3) [6], both for backbones) is consistent with the slow manifestation of the asymptotics. Indeed, fits over the initial ranges (right plot of Figure 4) yielded quite similar results, 0.6646(2) on the backbones and 0.6547(2) on full incipient clusters. In $2d$ our estimate is also smaller than those previously reported: $\bar{\nu}_{2d} = 0.775(2)$. However, in view of our findings for the $3d$ case, 10^3 steps may still not be sufficient for capturing the true asymptotic behavior. A more extensive $2d$ study is currently ongoing.

Sampling the quenched average of the number of conformations $\bar{Z}$ turned out to be difficult, as the underlying distribution has large deviations. In fact, it resembles a lognormal distribution, implying that simple random sampling of percolation clusters will underestimate the average for long chains. A better approach is therefore to focus instead on the average entropy $\overline{\ln Z}$. Here the distribution is approximately Gaussian, and we found that its variance increases linearly: $\sigma^2_{\ln Z} \sim A\,N$ with $A = 0.1667(3)$. $\bar{Z}$ can then be approximately obtained via

$$\bar{Z} \approx e^{\overline{\ln Z} + \sigma^2_{\ln Z}/2} = e^{\overline{\ln Z} + AN/2} \equiv \overline{Z_{\text{logn}}}, \tag{8}$$

when we assume the (log)normal distribution. In Figure 5, the average entropy per monomer on $3d$ clusters is plotted against the number of steps, besides the logarithm of $\overline{Z_{\text{logn}}}$ and the naively estimated average. The inset of the plots shows least-squares fits from two different scaling assumptions:

$$\overline{\ln Z}\,/N = \ln a/N + \ln \mu_0 + (\gamma - 1)\ln N/N \tag{9}$$

and

$$\overline{\ln Z}\,/N = \ln a/N + \ln \mu_0 (1 + bN^{-\zeta}). \tag{10}$$

As can be seen in the right plot of Figure 5, Eq. (9) (dotted curve), which assumes a scaling law like the right-hand side of Eq. (2) for $\overline{\ln Z}$, does not at all fit the data. By contrast, Eq. (10) (solid curve) fits perfectly for $b = 1.3(3)$, $\zeta = 0.48(3)$, and $\ln \mu_0 = 0.2715(3)$. Assuming Eq. (8), this then yields:

$$\bar{Z} \sim \bar{\mu}^{N(1+b/N^\zeta)}, \quad \bar{\mu} = e^{\ln \mu_0 + A/2} = 1.4260(6). \tag{11}$$
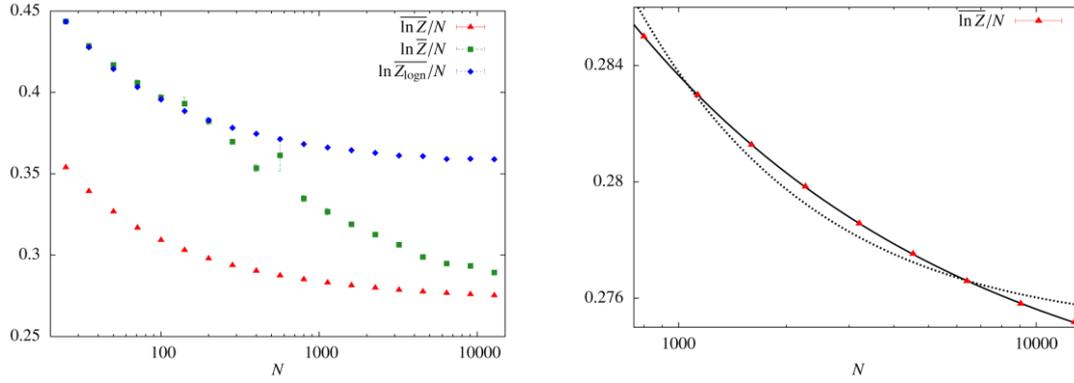
Figure 5: (left) Mean entropy (red triangles), logarithm of the average number of conformations (green squares), and log-normal approximation (blue diamonds) vs. N on a log-linear scale. The estimates for $\overline{\ln Z}$ are biased for $N > 200$ due to large deviations. (right) Fits of $\overline{\ln Z}$ using Eq. (9) (dotted) and Eq. (10) (continuous), respectively. Reproduced from Ref. [8].

For the $2d$ case, our preliminary analysis points to a similar behavior. These findings are very unexpected and still waiting to be explained by theory. We suspect that the factor $\bar{\mu}^{b/N^\zeta}$ is owed to the inhomogeneous spatial distribution of cluster regions that are entropically favorable, but the issue is still being investigated.

4 Semiflexible polymers in a quenched hard-disk fluid

We now turn to the conformational statistics of a grafted semiflexible polymer embedded in a quenched hard-disk fluid, which can be understood as a toy model for a biopolymer in the crowded cytoplasm of a cell. Every background realization adds to the WLC Hamiltonian (3) a potential energy term,

$$\mathcal{H} = \int_0^L \left[\frac{\kappa}{2} |\partial_s^2 \mathbf{r}(s)|^2 + V(\mathbf{r}(s)) \right] ds, \quad V(\mathbf{r}) = \sum_{i=1}^{\# \text{ disks}} \begin{cases} 0 & |\mathbf{R}_i - \mathbf{r}| > D/2 \\ \infty & \text{otherwise,} \end{cases} \tag{12}$$

where D denotes the disk diameter and $\mathbf{R}_i$ the respective disk positions. Due to the extreme strength and density of environmental interactions (the disorder filling fraction ranges from $\approx 40\,\%$ to $\approx 70\,\%$), this system is not amenable to standard Monte Carlo simulation techniques. However, it can be analyzed efficiently using a *growth algorithm* [21, 22, 23] that generates thermal equilibrium ensembles of semiflexible polymers by growing them outwards from their point of attachment as follows: (i) A large number Z of growth seeds are placed at the point of attachment $\mathbf{r}(0)$ and (ii) every growth seed is extended by one monomer pointing in a random direction. This generates a population of Z trial dimers, each of which is (iii) either deleted or replicated probabilistically such that the total population remains approximately constant and the average multiplicity of each configuration corresponds to its Boltzmann factor. Steps (ii) and (iii) are performed repeatedly until the polymers have reached the desired length L. We analyze the resulting equilibrium ensembles in terms of their length-averaged tangent-tangent correlation function

$$C(s) = \frac{1}{L-s} \int_0^{L-s} \overline{\langle \mathbf{t}(s_0 + s) \cdot \mathbf{t}(s_0) \rangle} \, ds_0 \tag{13}$$
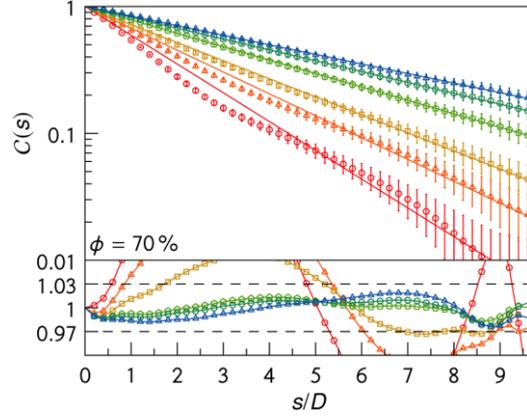
Figure 6: The numerically determined tangent correlations decay exponentially in the limit $\ell_p/D \to \infty$ (here shown for $\ell_p/D = 2, 3, 4, 6, 8, 10$ and a background filling fraction of 70 %), and decay more quickly for higher disorder filling fractions ϕ. The relative deviations of our exponential fits to the data are shown in the lower panel. Above $\ell_p = 6D$, these deviations nowhere exceed ≈ 3 %. Reproduced from Ref. [9].
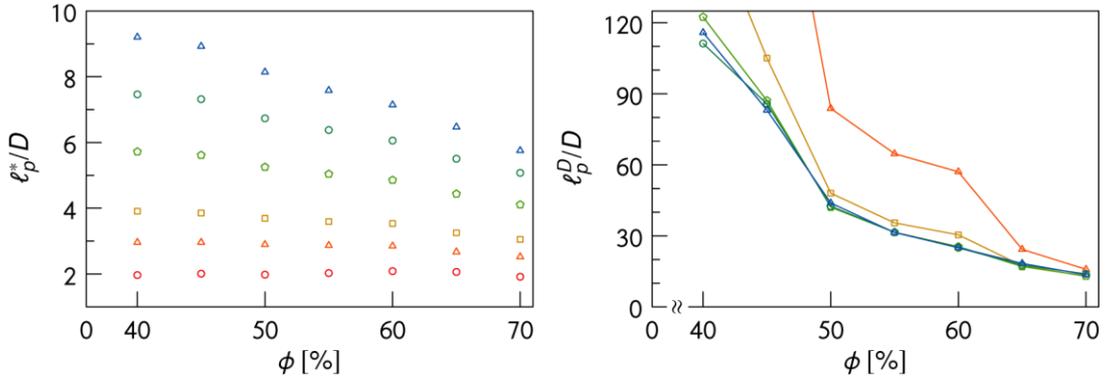
Figure 7: Left: Renormalized persistence length ℓ_p^* as function of the hard-disk fluid area filling fraction ϕ. Right: Disorder persistence length ℓ_p^D as determined via Eq. (18). Reproduced from Ref. [9].

and in terms of their radial end-to-end distribution function

$$\mathcal{P}(r) = 2\pi r \overline{\langle \delta(|\boldsymbol{r}(L) - \boldsymbol{r}(0)| - r)\rangle}, \tag{14}$$

where $\overline{\cdots}$ again denotes the quenched disorder average.

We find that, for sufficiently stiff polymers ($\ell_p \gtrsim 0.6L$), tangent correlations decay exponentially but with a renormalized persistence length ℓ_p^* that is significantly smaller than the thermal persistence length ℓ_p in free space (5), see Figures 6 and 7 [9].

A more sensitive observable is the radial end-to-end distribution $\mathcal{P}(r)$, which highlights local variations in the background field and thus picks up small-wavelength modulations that reflect the distribution of free volume within the surrounding hard-disk fluid. When multiplied by the "void space distribution function", a close cousin of the radial distribution function known from liquid-state theory,

$$g^{\text{void}}(r) \propto \frac{1}{r} \overline{\int \mathrm{d}^3 \boldsymbol{r}' \, \delta(|\boldsymbol{r}'| - r) e^{-\beta V(\boldsymbol{0})} e^{-\beta V(\boldsymbol{r}')}}, \tag{15}$$

the WLC radial distribution function $\mathcal{P}(r)$ evaluated for the renormalized persistence length ℓ_p^* is in good agreement with our numerical data, see Figure 8 [9].
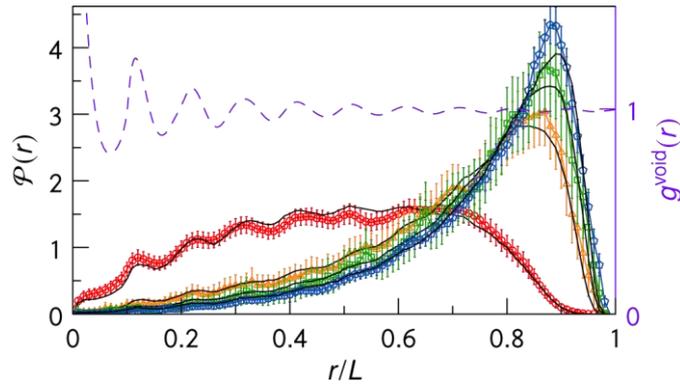
Figure 8: The renormalized persistence length ℓ_p^* can approximately account for the disorder-modulated radial distribution function $\mathcal{P}(r)$ (here shown for $\ell_p = 2D$ (red), $\ell_p = 6D$ (orange), $\ell_p = 8D$ (green), $\ell_p = 10D$ (blue)), if the renormalized WLC result is multiplied by the void space distribution function g^{void}. Reproduced from Ref. [9].

Interestingly, the renormalized persistence lengths ℓ_p^* observed for different values of the thermal persistence length ℓ_p collapse onto a single master curve ℓ_p^D under the following transformation,

$$\frac{1}{\ell_p^*} = \frac{1}{\ell_p} + \frac{1}{\ell_p^D}, \tag{16}$$

where the "disorder persistence length" ℓ_p^D depends only on the disorder filling fraction and thus provides a novel quantitative measure of molecular crowding.

5 Tube width statistics

As an alternative approach to the problem of the statistical conformation of a biopolymer in the crowded environment of the cytoplasm, we consider the tube model for semiflexible polymers [12]. In contrast to the above, the disorder background is here not externally prescribed as a quenched field but instead emerges self-consistently from the interaction of the test polymer with identical surrounding polymers in a polymer solution. Furthermore, it is not a consequence of volume exclusion but of the thermal fluctuations of the chains (that can be imagined as infinitely thin lines) and the topological restriction that they cannot cross each other.

We tackle the topological many-body problem of the polymer solution by a binary collision approach designed for purely steric interactions. The free energy $\mathcal{F}_\pm(\boldsymbol{h})$ of confinement due to the uncrossability of the chains is associated to each pair collision and locally identified with the mean harmonic tube potential introduced in Eq. (6). Here, $\boldsymbol{h}$ denotes the displacement of the test polymer's preferred contour, which is approximated by a straight line, and the subscript $\pm$ refers to the entanglement topology, specifying whether the colliding polymers can be continuously transformed into ground states without intersection or not. This allows for a self-consistent determination of the tube strength

$$\varphi_\pm = \partial_h^2 \mathcal{F}_\pm(\boldsymbol{h})|_{h=0} \tag{17}$$

as a function of the actual network configuration, which is characterized through the distance of the preferred contours and the entanglement topology of the two colliding polymers. Within the binary collision scheme, we neglect correlations of the collisions along the chain and approximate the local
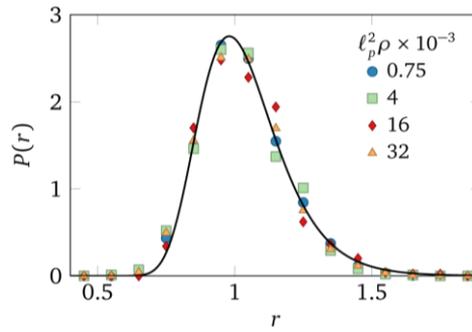
Figure 9: Tube size distribution obtained from the binary collision approximation (solid line), Eq. (18), compared to hybrid Monte Carlo / Brownian dynamics simulations (symbols) by Ramanathan and Morse [24] for a concentration range (ρ is the polymer length per volume) comparable to that realized in typical experimental systems. In the simulations, the tube size is measured after a characteristic time interval at which the growth of the polymers' transverse MSD slows down.

entanglement segment by a homogeneous cylinder with its length given by the characteristic distance between collisions along a chain, the so-called entanglement length [11]. Within this segment fluid approach, which generalizes the conventional tube model [12], the ensemble of possible network configurations gives rise to a distribution $P(\varphi)$ of the local tube strength, which we translate into the tube size distribution $P(r)$. It can be computed within the outlined analytical approximation as

$$P(r) = c \exp(-6.76r^{-8/3})r^{-6.76\times 8/3 - 1},\qquad(18)$$

where c is a normalization constant and r denotes the tube radius scaled by its mean $\langle r\rangle$. Our approach thus predicts a universal shape of $P(r)$ that does not depend on the polymer concentration. This property and the shape of $P(r)$, characterized by a positive skewness and a broad tail at large r, was found to be in excellent agreement with experimental data gained from the F-actin solutions, as shown in Ref. [10]. In Figure 9, we test (18) against tube size distributions obtained from hybrid Monte Carlo / Brownian dynamics simulations proposed by Ramanathan and Morse [24] to simulate networks of entangled wormlike chains that have zero thickness but cannot cross each other. In the underlying algorithm, trial moves of the bead-stick polymers are computed from a numerically integrated Langevin equation. It was shown in Ref. [24], how the increase of the mean square deviation (MSD) of the transverse polymer fluctuations slows down after a characteristic time interval, indicating that the average polymer in the simulation has explored its whole tube. When measured at this so-called entanglement time, $P(r)$ is indeed well described by the binary collision approximation of Eq. (18).

6   Summary and conclusions

The self-avoiding random walk on a fractal percolation cluster serves as a paradigmatic model system for flexible polymers subject to scale-free disorder. Using a newly developed exact enumeration algorithm, we have determined its mean square end-to-end extension to unprecedented precision and showed that its partition sum is subject to a different scaling law than hitherto assumed.

Employing an efficient stochastic growth algorithm, we simulated semiflexible polymers exposed to statistically isotropic, quenched steric disorder and found them to exhibit effective WLC statistics, but with a renormalized persistence length. We empirically discovered a simple relation between this renormalized persistence length and the thermal persistence length, which defines a novel quantitative

measure of molecular crowding and allows us to use semiflexible polymers as a local probe of material microstructure.

We furthermore generalized the classical tube model for semiflexible polymers to a "segment fluid model" that resolves local tube width fluctuations. Based on this model, we were able to derive a universal distribution of tube radii that reflects the intrinsically disordered nature of semiflexible polymer networks and is in good agreement with experimental data.

Acknowledgements

References

[1] R. Ellis: *Macromolecular crowding: Obvious but underappreciated*. Trends Biochem. Sci. **26**, 597–604 (2001)

[2] Y.-L. Sun, Z.-P. Luo, A. Fertala, K.-N. An: *Stretching type II collagen with optical tweezers*. J. Biomech. **37**, 1665–1669 (2004)

[3] D.A. Fletcher, R.D. Mullins: *Cell mechanics and the cytoskeleton*. Nature **463**, 485–492 (2010)

[4] K. Barat, B.K. Chakrabarti: *Statistics of self-avoiding walks on random lattices*. Phys. Rep. **258**, 377–411 (1995)

[5] A. Ordemann, M. Porto, H.E. Roman, S. Havlin, A. Bunde: *Multifractal behavior of linear polymers in disordered media*. Phys. Rev. E **61**, 6858–6865 (2000)

[6] V. Blavatska, W. Janke: *Scaling behavior of self-avoiding walks on percolation clusters*. Europhys. Lett. **82**, 66006 (2008)

[7] N. Fricke, W. Janke: *Scale-free enumeration of self-avoiding walks on critical percolation clusters*. Europhys. Lett. **99**, 56005 (2012)

[8] N. Fricke, W. Janke: *Asymptotic scaling behavior of self-avoiding walks on critical percolation clusters*. Phys. Rev. Lett. **113**, 255701 (2014)

[9] S. Schöbl, S. Sturm, W. Janke, K. Kroy: *Persistence-length renormalization of polymers in a crowded environment of hard disks*. Phys. Rev. Lett. **113**, 238302 (2014)

[10] J. Glaser, K. Kroy: *Fluctuations of stiff polymers and cell mechanics*. In *Biopolymers*, ed. M. Elnashar, chapter 26, InTech (2010)

[11] J. Glaser, K. Kroy: *Tube-width fluctuations of entangled stiff polymers*. Phys. Rev. E **84**, 051801 (2011)

[12] D.C. Morse: *Tube diameter in tightly entangled solutions of semiflexible polymers*. Phys. Rev. E **63**, 031502 (2001)

[13] P. Grassberger: *Pruned-enriched Rosenbluth method: Simulations of θ polymers of chain length up to 1 000 000*. Phys. Rev. E **56**, 3682–3693 (1997)

[14] N. Fricke, W. Janke: *Self-avoiding walks on strongly diluted lattices: Chain-growth simulations vs. exact enumeration*. Eur. Phys. J. Spec. Top. **216**, 175–179 (2013)

[15] A.R. Singh, D. Giri, S. Kumar: *Effects of molecular crowding on stretching of polymers in poor solvent*. Phys. Rev. E **79**, 051801 (2009)

[16] D. Ben-Avraham, S. Havlin: *Diffusion and reactions in fractals and disordered systems*. Cambridge University Press, Cambridge (2000)

[17] N. Fricke, W. Janke: *How to enumerate 10^{1000} self-avoiding walks on a critical percolation cluster*. In preparation

[18] N. Fricke, W. Janke: *Self-attracting self-avoiding walks on critical percolation clusters*. In preparation

[19] R. Rammal, G. Toulouse, J. Vannimenus: *Self-avoiding walks on fractal spaces: Exact results and Flory approximation*. J. Phys. (Paris) **45**, 389–394 (1984)

[20] K.Y. Woo, S.B. Lee: *Monte Carlo study of self-avoiding walks on a percolation cluster*. Phys. Rev. A **44**, 999–1007 (1991)

[21] T. Garel, H. Orland: *Guided replication of random chain: A new Monte Carlo method*. J. Phys. A **23**, L621–L626 (1999)

[22] S. Schöbl, J. Zierenberg, W. Janke: *Simulating flexible polymers in a potential of randomly distributed hard disks*. Phys. Rev. E **84**, 051805 (2011)

[23] S. Schöbl, J. Zierenberg, W. Janke: *Influence of lattice disorder on the structure of persistent polymer chains*. J. Phys. A **45**, 475002 (2012)

[24] S. Ramanathan, D.C. Morse: *Brownian dynamics algorithm for entangled wormlike threads*. J. Chem. Phys. **126**, 094906 (2007)